Mesoporous Carbon Materials Improving Li-O_2 Batteries Cathode Performances by its Permselective Channels

Undergraduate Research Opportunities in Science

PROJECT REPORT

Submitted by

Li Zeng

A0197647J

Supervised by

Assoc. Prof. Chen, Wei

Department of Chemistry

National University of Singapore

CM3289 (8MC)

September, 2019

(3235 words)

Content

Abstract

Improving the life time of batteries is one of the most challengable problem. One way to pursue good cycling performance lithium-oxygen (Li_2O_2) batteries is to achieve low charge overpotentials. Here, ordered mesoporous carbon materials (CMK-8) are rationally designed as an oxygen cathode for Li-O_2 batteries to reduce the charge overpotential then lengthen the cycle life. Due to the ordered mesoporous features, CMK-8 not only can provide abundant channels for the transportation of Li^+ and O_2 by the capillary force, but also serves a block to prohibit lithium superfoxide (LiO_2) being diffused during the oxygen reduction reaction (ORR) process due to the unique cubic Ia3d structure. Therefoer, Amorphous lithium peroxide (Li_2O_2) can form in the pore interiors of CMK-8. Such designed catalysts enable excellent electrochemical performances due to the improved conductivity in amorphous Li_2O_2 as well as the good Li_2O_2/CMK-8 contact interface. Finally, at a current density of 0.1 A g^{-1}, the CMK-8 electrode can deliver a low charge overpotential of 0.43 V without any obvious degradation even after 45 cycles with a limited capacity of 500 mAh g^{-1}.

1. Introduction

How to solve the exhausting gas is one of the problems in air pollution purification field. Scientists and engineers have proposed to replace classic cars with electric vehicles, since concentrated exhausting gas could be easilier purified than the gas from individual cars. Recently, main-stream electric vehcles are using lithium-ion batteries (LIBs) as the energy supplier[1,2]. Comparing with the LIBs, the lithium-oxygen battery, a new type of battery, is designed to break through the limit of the LIBs with high theoretical specific energy (energy per unit mass), 3,500 Wh kg^{-1} [3,4]. In practice, such a high value cannot be gotten due to many factors, but values could be in a range between 500 and 1,000 Wh kg^{-1}. It is a sufficient amount of energy to support an electric vehicle in excess of a 500 km driving range. However, Li-O_2 batteries also face some challenges, such as life time as well as energy efficiency[5,6]. In fact, these things could be influenced by several parts of the battery-cathode, anode, electrolyte and so on. For example, the low coulombic and energy efficiency can be caused by the insulating discharge products of lithium peroxide (Li_2O_2), which also leads to a significantly high charge overpotential and further affects the life time of the batteries. Besides, related parasitic reactions between Li_2O_2 and solvents would aggravate the decreasing of energy efficiency as well as degrading of the batteries cycle life[7].

The main objective of this article aims at how to lengthen the cycling performance. To achieve this, reducing the charge overpotential is a critical point. Various liquid and solid catalysts have been applied[8-13]. Each one has its own benefits. Here, we focused onto the solid catalysts. In this case, the direct contact between lithium peroxide and catalysts

interface is usually required for the surface reaction mechanism. If such contact is interrupted, catalytic effect would be ceased[14,15]. Besides, crystalline Li_2O_2 has low conductiveity and further causes a comparably high charge overpotential, leading to a low energy efficiency and poor cycle life battery[7,16].

Hence, controlling the growth of amorphous Li_2O_2 with the good Li_2O_2/catalyst contact could enhance the electrochemical performance. It can be achieved by controlling the growth models of Li_2O_2, i.e. the solution model and the surface model[17,18]. These growth models are maily controlled by tuning the solubility of lithium superoxide (LiO_2) intermediates[19]; therefore, it is needed to develop a sort of cathode which can guide the amorphous Li_2O_2 growth from LiO_2 with contrable solubility in the intrinsic channels of solid catalysts. Moreover, such a design should also provide sufficient channels for the transportation of O_2 and Li^+, while the LiO_2 intermediates dissolution is simultaneously inhibited, forming amorphous Li_2O_2 in the pore channels. In this work, we designed the ordered mesoporous carbon materials (CMK-8) as the cathode. It finds that ordered mesopores can be permselevtive only for Li^+ and O_2 transportation due to the capillary force but impenetrable for LiO_2 during the oxygen reduction reaction (ORR) owing to the unique cubic Ia3d structure. Thereby, the amorphous Li_2O_2 can be effectively trapped in the channel interiors. The improved conductivity in amorphous Li_2O_2 and the favorable Li_2O_2/CMK-8 contact interface cause a low charge overpotential. As expected, the battery with the CMK-8 cathode possesses a low charge overpotential of 0.43 V without obvious performance degradation for 45 cycles at a current density of 0.1 A g^{-1} with a limited capacity of 500 mAh g^{-1}, far better than that of the cell with the EC-300J cathode.

2. Materials and Methods

2.1. Preparation of CMK-8

Incipient wetness mehod was applied to make the CMK-8. By setting KIT-6 (3.0 g) as a template, 80% of the pore volume of KIT-6 was impregnated by the added furfuryl alcohol. Next, the impregnated KIT-6 was dried at 110 °C for two hours and then heated at 350 °C for two hours in a tube furnace under N_2 atmosphere with a heating rate of 2 °C/min. This process should be repeated twice and the volumes of furfuryl alcohol would then approximately correspond to 50% and 20% of the pore volume of KIT-6, respectively. After these three impregnation steps, the mixture was carbonized at a temperature of 750 °C for two hours in N_2 flow. To obtain pure CMK-8, the black carbonized powder would be washed with 2 M NaOH and deionized water to remove the residual silica template. Finally, the powder was dried at 100 °C for twelve hours to obtain pure CMK-8[20].

2.2. Preparation of f-CMK-8

For the chemical modification of the CMK-8 surfaces, the CMK-8 (3 g) was refluxed in HNO_3 (90 mL, 65 wt%) at 120 °C for 5 h, followed by washing thoroughly with DI water and dried at 60 °C to achieve f-CMK-8[21].

2.3. Characterizations

HR-TEM (TEM, FEI Titan 80<300), FE-SEM (JEOL JSM-6700F), and N_2 adsorption-desorption analysis (NOVA 2200e) were used to analyze the structural and morphological information of involved samples. XRD measurements were conducted on a PANalytical

Empyren DY 708 diffractometer based on CU radiation (Cu Kα=0.15406 nm). Raman spectra were performed from Renishaw inVia 2000 with a laser exciting wave length of 532 nm.

2.4. Test Cells Assembly

The catalyst was prepared by adding cathode materials (CMK-8 or EC-300J, 90 wt%) and a poly (vinylidene fluoride) (PVDF, 10 wt%) binder, and then the catalyst slurry was dispersed into 1-methyl-2 pyrrolidone (NMP), followed by coating the slurry on the carbon paper collectors with a film thickness of 50 μm. The oxygen cathodes were dried in an oven at 100 ºC for twlve hours. The discharge capacity was calculated by the weight of the catalysts, and the catalyst loading on the carbon paper was 0.5-1 mg cm^{-2}. By using coin cells (2032), the Li-O_2 batteries were assembled in a glovebox under argon atmosphere, including a Li metal anode, 1 M lithium trifluoromethanesulfonate/tetraethylene glycol dimethyl ether ($LiCF_3SO_3$/TEGDME) electrolyte within a glass fiber separator, and an oxygen cathode.

2.5. Electrochemical measurements

The galvanostatic discharge-charge tests of the Li-O_2 batteries were conducted on an LAND testing system within a voltage window of 2.0-4.5 V. The EIS and CV were measured from a Bio-logic AUTOLAB electrochemical station. The amplitude and frequency range of EIS measurements were set to be 5 mV and 10^5-10^{-2} Hz, respectively, and the scanning rate of CV was set to be 0.03 mVs^{-1} between 2.0 and 4.5 V. A Swagelok

type of Li-O_2 batteries were connected to two PEEK capillary tubes for in-situ DEMS measurements. For discharge process, a mixed gas of O_2/Ar (4:1) was used as the working gas to identify O_2 consumption. For charge process, Ar acted as carrier gas to observe the O_2 evolution.

3. Results and Discussion

3.1. Characterization of CMK-8.

Due to the pore structures, CMK-8 could be investigated by high-resolution transmission electron microscopy (HR-TEM). As shown in Figure 1(a), produced CMK-8 exihibited ordered mesporous channels with pore diameters at around 4.2 nm, which was detected by the lattice fringe distance as the spacing between two yellow lines. In the low-angle X-ray diffraction (XRD) pattern (Figure 1(b)), there were three apparent diffraction peaks, indexed as the (211), (220), and (420) planes. Here (211) and (220) planes can reveal a highly ordered cubic Ia3d structure[22], and according to Bragg's law, (420) plane exactly corresponded to the lattice fringe spacing of 4.2 nm. Besides, the adsorption/desorption isotherm (Figure 1(c)) plus the Barrett-Joyner-Halenda (BJH) pore distribution (Figure 1(d)) by the adsorption branch from the Figure 1(c) were presented. According to these two results, produced CMK-8 can be detected that it possesses a high specific surface area (687 m^2g^{-1}) and a large pore volume (0.99 cm^3g^{-1}) due to the abundant mesoporous features. Additionally, as shown in Figure 1(d), the mesopores centered at around 3.4 nm (indirectly calculated) was consistent with the HR-TEM result (4.2 nm) in Figure 1(a). Both 3.4 nm and 4.2 nm are in the range of 3~4 nm as shown in others' work[23]. Hence,

CMK-8 was successfully produced and could be applied in the following test.

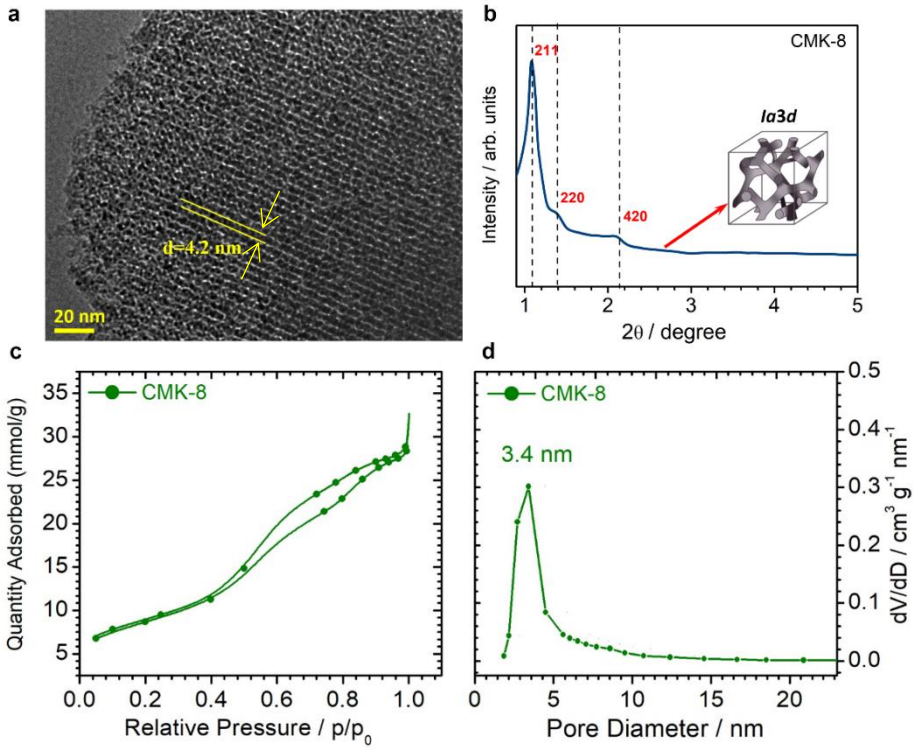

Figure 1. Characterization of Produced CMK-8 (a) HR-TEM image, (b) XRD pattern, (c) the adsorption/desorption isotherm, (d) the pore size distribution of CMK-8.

3.2. Discharge-charge process of Li-O_2 batteries with CMK-8 cathode

Since prepared CMK-8 was same as other researchers', it was assembled in Li-O_2 batteries (see 2.3. Test batteries assembly) , and thoses batteries were tested. The discharge-charge profile of batteries was shown in Figure 2(a). The hypothesis of this research was that constructed pore channels of CMK-8 could be permselective to allow the transportation of Li^+ and O_2 but Li_2O_2. Therefore, TEM were applied to detect whether the discharge product Li_2O_2 particles were locked in the pores. Figure 2(b)-(f) confirmed that the Li_2O_2 gradually impregnated the mesoporous channels of the CMK-8 electrode with continuous discharge processes, as shown in Figure (b)-(d). However, such images could also be detected if Li_2O_2 was grown onto the surface of cathode. To exclude this

possibility, functionalized CMK-8 (f-CMK-8, see the Appendex) was prepared to facilitate and simulate the surface growth model of the Li_2O_2 film forming onto the surface[24]. The distinct morphologies of discharge products of CMK-8 and f-CMK-8 confirmed that the Li_2O_2 was indeed grown in the pore interiors of CMK-8 cathodes. In addition, after recharging to 1000 mAh g^{-1}, the CMK-8 cathode (Figure 2(f)) recovers to its initial state (Figure 2(b)), indicating the complete decomposition of Li_2O_2, and good reversibility of Li-O_2 batteries with the CMK-8 cathode.

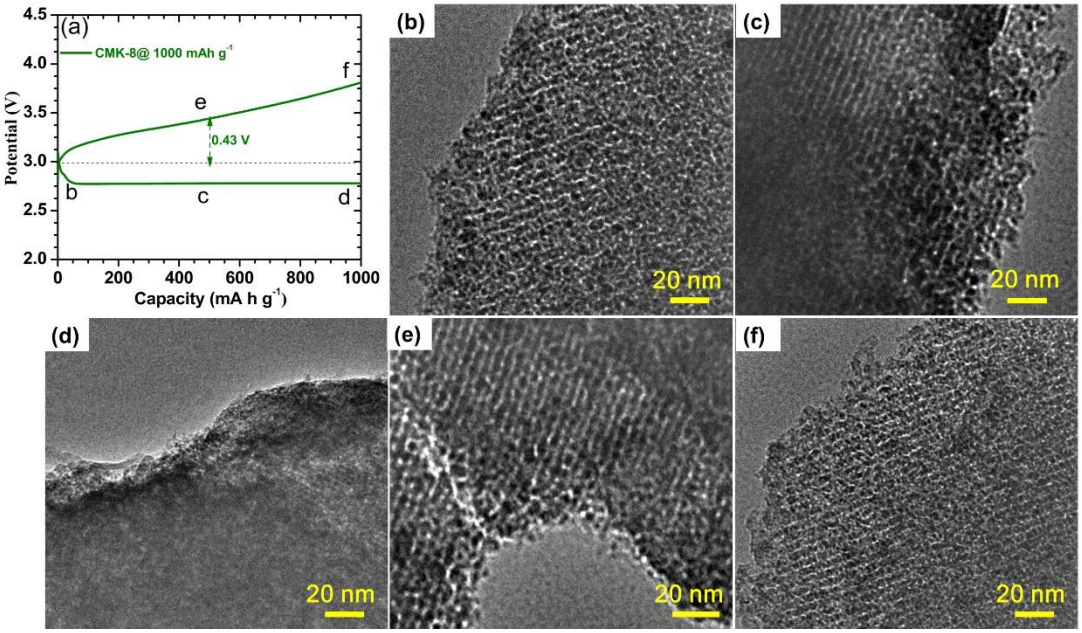

Figure 2. (a) The discharge-charge profies of Li-O_2 batteries with the CMK-8 cathode at a current density of 0.1 A g^{-1} with a limited capacity of 1000 mAh g^{-1} for the first cycle; (b)-(f) TEM images of the CMK-8 cathode taken at each typical point in (a)

3.3. Overpotential comparisons between CMK-8 and EC-300J

CMK-8 was successfully produced with mesoporous channels constructure and Li_2O_2 was confirmed growing in the channels. It was necessary to do the cell tests and compare CMK-8 cahode with another cathode made of common materials in Li-O_2 batteries -- EC-300J. In Figure 3(a), the discharge-charge profiles of both CMK-8 and EC-300J cathodes

were evaluated at 0.1 A g^{-1} with a limited capacity of 500 mAh g^{-1}. The battery using CMK-8 cathode exihibit a lower charge overpotential of 0.43 V comparing with that of EC-300J cathode (1.16 V). Meanwhile, the low charge overpotential of the CMK-8 cathode can also be obviously reflected by the cyclic voltammograms (CVs) results, as shown in Figure 3(b). At a constant scanning rate of 0.03 mV s^{-1}, despite an approximate ORR peak (around 2.29 V) of the cells with CMK-8 and EC-300J cathodes, the cell with the CMK-8 cathode exhibits a low anodic peak of 3.46 V compared to that of the EC-300J-based cell, which is consistent with the charge curve in Figure 3(a). Furthermore, the sweep areas of the CMK-8 cathode significantly increased during oxygen evolution reaction (OER) compared to that of the EC-300J cathode (Figure 3(b)), revealing that the CMK-8 cahtode exhibits superior electrochemical performance in the decomposition of the discharge product.

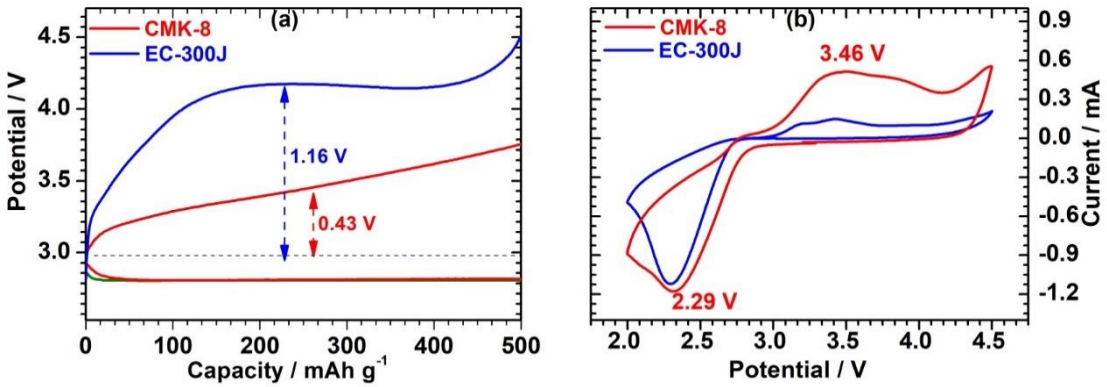

Figure 3. (a) Discharge-charge curves of Li-O_2 batteries with CMK-8 and EC-300J cathodes with a limited capacity of 500 mAh g^{-1} for the 1st cycle; (b) CVs of Li-O_2 batteries with CMK-8 and EC-300J cathodes at a scan rate of 0.03 mV s^{-1} in the voltage range of 2.2-4.5 V vs. Li^+/Li for the 1st cycle.

3.4. Exact discharge product of CMK-8 cahode

Although the discharge product of Li-O_2 batteries with EC-300J cathode is Li_2O_2 film,

CMK-8 cathode was constructed to cubic mesoporous structure; hence, the morphologies of discharge product may be changed. When XRD measurement was applied at the beginning, for the control group: EC-300J, it was obvious to see the corresponding peaks of crystalline Li_2O_2, at 32.9°, 35°, and 58.68° (Figure 4(a)) However, those three peaks did not appear in the XRD pattern of CMK-8 cathode. Moreover, the XRD pattern of CMK-8 cathode did not exhibit any peak could correspond with crystallines of LiOH, Li_2CO_3 or any other related Li reaction product. To examine the exact discharge product of CMK-8 cathode, Raman spectroscopy was further applied. As shown in Figure 4(b), the peak at 788 cm^{-1} arising from the strtching vibration of LiO-OLi[25] can be detected on both EC-300J and CMK-8 cathodes, indicating that the discharge products were Li_2O_2. Nevertheless, the peak of LiO-OLi stretching of CMK-8 at 789 cm^{-1} was less than the half maximum, and the Li-O lattice vibration peak at 258 cm^{-1} was absent on the CMK-8 cathode. Therefore, the discharge product in CMK-8 cathode was not crystalline Li_2O_2; instead, it was amorphous Li_2O_2.

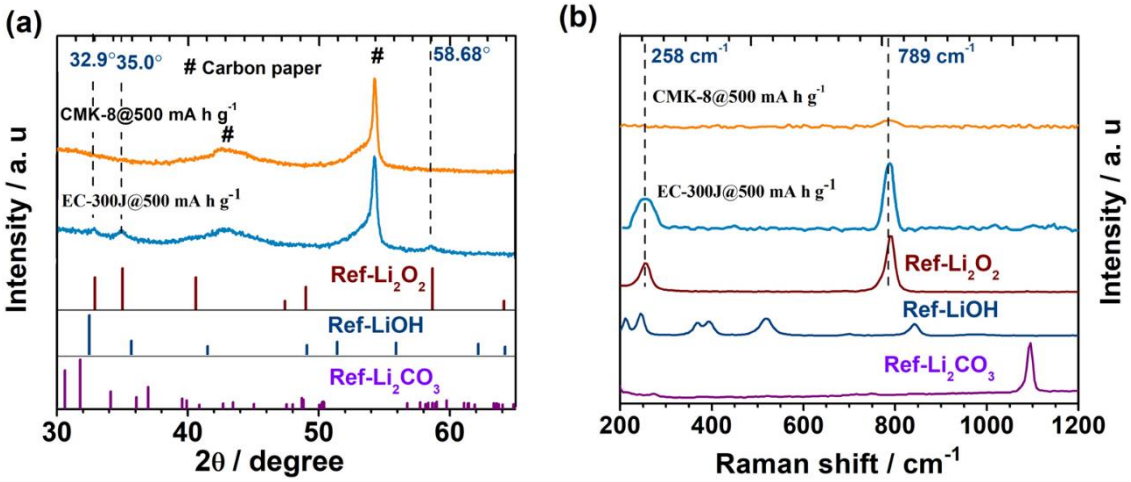

Figure 4 (a) XRD patterns and (b) Raman spectra for the EC-300J and CMK-8 cathodes after 1st discharge with a limited capacity of 500 mAh g^{-1}

3.5. Good reversibility and stability of the batteries with CMK-8 cathode

Quantitative differential electrochemical mass spectrometry (DEMS) provided the *in-situ* measurements of the O_2 consumption/evolution during the discharge-charge processes. As shown in Figure 5(a)-(b), during the discharge processes of both cathode, only O_2 is consumed and the molar ratios of electrons to the consumed O_2 were 2.04 and 2.07, respectively, suggesting that the main discharge reaction product was Li_2O_2 for both CMK-8 and EC-300J cathode since the e^-/O_2 of reactions was nearly two. It is consistent with the results of XRD measurments and Raman spectroscopy in section 3.4. Nonetheless, the charging processes of these two cells were significantly different. In Figure 5(c)-(d), during the charging processes, the ratio of e^-/O_2 of CMK-8 cathode kept stable at 2.05, while that of EC-300J cathode was not so stable with higher value (2.37). In addition, CO_2 evolution could be detected during the charge process of EC-300J cathode, and the charge line had a plateau when the ratio of e^-/O_2 suddenly increased (O_2 evolution decreased). These unstable lines in Figure 5(d) corroborated that there were side reactions occurring during the charge process of EC-300J cathode; in other words, CMK-8 electode could effectively suppress the side reactions, leading a superior

electrochemical stability and reversibility.

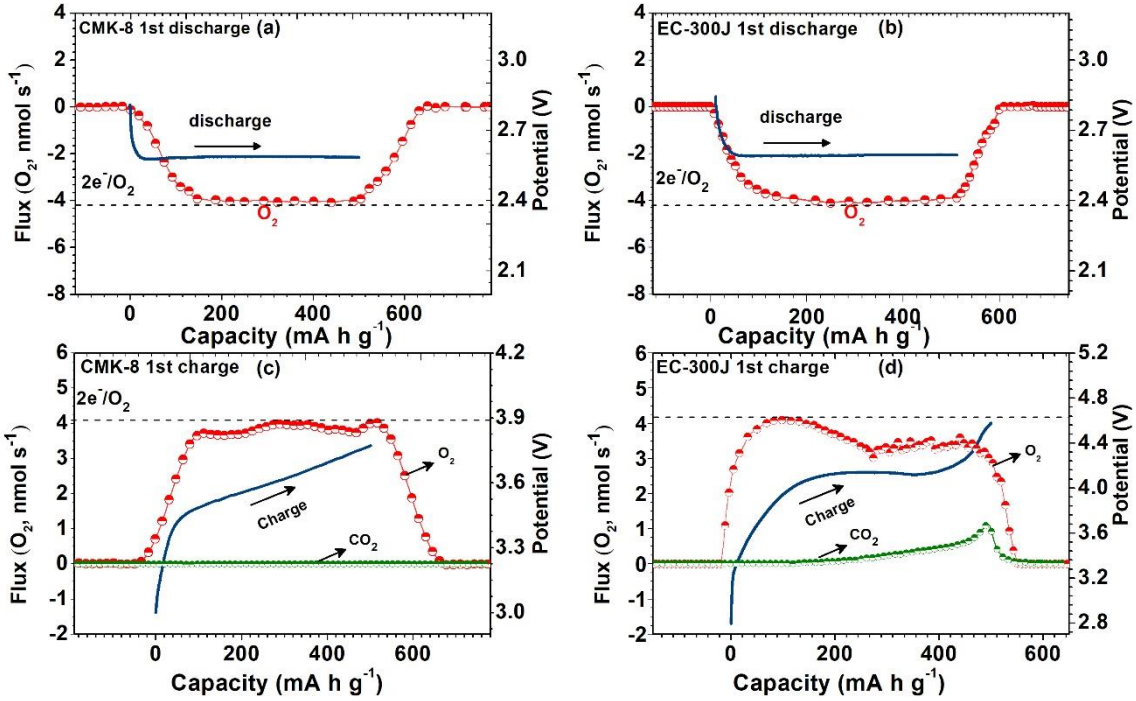

Figure 5. DEMS results of Li-O_2 batteries with (a, c) CMK-8 and (b, d) EC-300J cathodes for the 1st (a, b) discharge and (c, d) charge process at a current of 0.8 mA (current density: 0.1 A g^{-1}) with a limited capacity of 500 mA g^{-1}.

3.6. Cycling performance of CMK-8 cathode

As mentioned in the introduction, the final objective of this research is to enhance the life time of the Li-O_2 batteries. From Figure 6(a), the CMK-8 cathode could achieve 45 cycles at 0.1 A g^{-1} with a limited capacity of 500 mAh g^{-1}, and the charge overpotential remained at around 0.45 V without any obvious degradation. This was due to the negligible side reactions as the result of section 3.5. Actually, in Figure S2, it was noted that after 75 cycles, the charge overpotential increased to 1.0 V due to the corrosion of the Li metal anode by the O_2 crossing electrolyte forming LiOH (Figure S3). Therefore, when the corrosed Li metal anode was replaced by a new one, the battery with the same CMK-8 cathode and electrolyte could be reversibly cycled for another 40 times again. By contrast,

the batteries with EC-300J cathode could only be operated for 20 cycles with a remarkable increase of discharge-charge overpotentials (Figure 6(b)) owing to side reactions (see section 3.5.). Besides, according to the electrochemical impedance spectroscopy (EIS) analysis, the electrochemical performance stability of the CMK-8 as well as EC-300J cathode could be detected, as shown in Figure 6(c)-(d). Here, R_s, R_{ct1} and R_{ct2} represented the solvent resistance, the electrolyte-electrode interface resistance, and the electrochemical polarization resistance, respectively; as for CPE, C and Z_w separately standed for the consan-phase element, the double layer capacitances, and the Warburg impedance. For the EC-300J-based batteries, the incomplete decomposition of Li_2O_2 and the side product (Li_2CO_3) were detected by the XRD pattern (Figure S4) after 15 cycles. This resulted in a sharp increase of R_{ct1} and R_{ct2}; thereby leaded to the poor cycling performance. In contrast, because of the negligible side products (Figure S6), the CMK-8-based batteries displayed a slight variation of R_{ct1} and R_{ct2} after 15 cycles. This comparison could be seen in the Figure 6(c)-(d) , and suggested that the parasitic side reactions were greatly suppressed by CMK-8 cathode, consistent with the DEMS result in section 3.5.

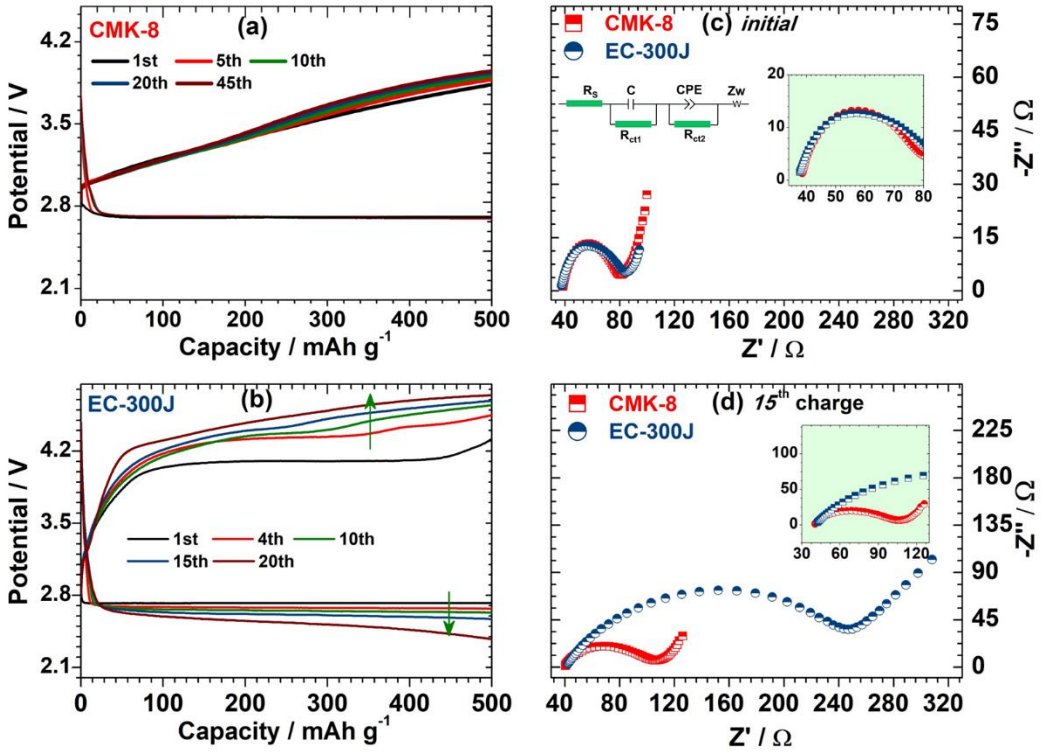

Figure 6. (a)-(b) The cycling performance of the Li-O_2 batteries with (a) EC-300J and (b) CMK-8 cathodes at a current density of 0.1 A g^{-1} with a limited capacity of 500 mAh g^{-1}; (c)-(d) the Nyquist plots of EC-300J and CMK-8 cathodes for (c) fresh cells and (d) charged cells after 15 cycles.

4. Conclusion

In summary, the CMK-8 has been employed as oxygen cathode for Li-O_2 batteries and successfully increased the life time of the battery. Benefiting from its unique cubic network fram (Ia3d), CMK-8 could retain amorphous Li_2O_2 particles by the impenetrable pores for LiO_2, which will then form Li_2O_2. This would also reduce the side reactions to tablize the whole reaction process. Due to the trapped Li_2O_2 in the pore interiors, the conductiveity of Li_2O_2 will be increased by the good Li_2O_2 / CMK-8 contact interface leading to a low charge overpotential and excellent life expectancy. According to the performance test, decreasing the overpotential to 0.46 volts (reduced by 0.67 volts comparing with EC-300J cathode) at a current density of 0.1A g^{-1} without obvious

influence after 45 cycles with a limited capacity of 500 mAh g^{-1}. That demonstrats a gree potential of lithium-oxygen batteries.

Reference

1 Bert Metz, O. D., Heleen de Coninck, Manuela Loos, and Leo Meyer. . *IPCC special report on carbon dioxide capture and storage*. (United States: N. p., 2005).

2 2018 Outlook for Energy: A View to 2040. 1-62 (Exxon Mobil Corporation, 2018).

3 K.M.Abraham & Jiang, Z. A polymer electrolyte-based rechargeable lithium-oxygen battery. *J. Electrochem. Soc.* **143**, 1-5 (1996).

4 Ogasawara, T., Debart, A., Holzapfel, M., Novak, P. & Bruce, P. G. Rechargeable Li_2O_2 electrode for lithium batteries. *Journal of the American Chemical Society* **128**, 1390-1393 (2006).

5 Wang, Z., Sun, J., Cheng, Y. & Niu, C. Adsorption and deposition of Li_2O_2 on TiC{111} surface. *J. Phys. Chem. Lett.* **5**, 3919-3923 (2014).

6 Muhammed M. Ottakam Thotiyl, S. A. F., Zhangquan Peng, Yuhui Chen, Zheng Liu and Peter G. Bruce. A stable cathode for the aprotic Li–O_2 Battery. *Nature Materials* **12**, 1050-1056 (2013).

7 Aurbach, D., McCloskey, B. D., Nazar, L. F. & Bruce, P. G. Advances in understanding mechanisms underpinning lithium–air batteries. *Nature Energy* **1**, doi:10.1038/nenergy.2016.128 (2016).

8 Chen, Y., Freunberger, S. A., Peng, Z., Fontaine, O. & Bruce, P. G. Charging a Li-O_2 battery using a redox mediator. *Nature chemistry* **5**, 489-494, doi:10.1038/nchem.1646 (2013).

9 Yu, M., Ren, X., Ma, L. & Wu, Y. Integrating a redox-coupled dye-sensitized photoelectrode into a lithium-oxygen battery for photoassisted charging. *Nature communications* **5**, 5111, doi:10.1038/ncomms6111 (2014).

10 Feng, N., He, P. & Zhou, H. Enabling catalytic oxidation of Li_2O_2 at the liquid-solid interface: the evolution of an aprotic Li-O_2 battery. *ChemSusChem* **8**, 600-602, doi:10.1002/cssc.201403338 (2015).

11 Zhang, Z. *et al.* Identification of cathode stability in Li–CO_2 batteries with Cu nanoparticles highly dispersed on N-doped graphene. *Journal of Materials Chemistry A* **6**, 3218-3223, doi:10.1039/c7ta10497a (2018).

12 Sun, B., Huang, X., Chen, S., Munroe, P. & Wang, G. Porous graphene nanoarchitectures: an efficient catalyst for low charge-overpotential, long life, and high capacity lithium-oxygen batteries. *Nano letters* **14**, 3145-3152, doi:10.1021/nl500397y (2014).

13 Jian, Z. *et al.* Core-shell-structured CNT@RuO_2 composite as a high-performance cathode catalyst for rechargeable Li-O_2 batteries. *Angewandte Chemie* **53**, 442-446, doi:10.1002/anie.201307976 (2014).

14 Feng, N., He, P. & Zhou, H. Critical Challenges in Rechargeable Aprotic Li-O_2 Batteries. *Advanced Energy Materials* **6**, 1502303, doi:10.1002/aenm.201502303 (2016).

15 Zhang, J. *et al.* A versatile functionalized ionic liquid to boost the solution-mediated performances of lithium-oxygen batteries. *Nature communications* **10**, 602, doi:10.1038/s41467-019-08422-8 (2019).

16 Dutta, A. *et al.* Nanostructuring one-dimensional and amorphous lithium peroxide for high round-trip efficiency in lithium-oxygen batteries. *Nature communications* **9**, 680, doi:10.1038/s41467-017-02727-2 (2018).

17 Lyu, Z. *et al.* Recent advances in understanding of the mechanism and control of Li_2O_2

formation in aprotic Li-O_2 batteries. *Chemical Society reviews* **46**, 6046-6072, doi:10.1039/c7cs00255f (2017).

18 Lim, H. D. *et al.* Reaction chemistry in rechargeable Li-O_2 batteries. *Chemical Society reviews* **46**, 2873-2888, doi:10.1039/c6cs00929h (2017).

19 Lyu, Z. *et al.* Effect of oxygen adsorbability on the control of Li_2O_2 growth in Li-O_2 batteries: Implications for cathode catalyst design. *Nano Energy* **36**, 68-75, doi:10.1016/j.nanoen.2017.04.022 (2017).

20 Phan, T. N., Gong, M. K., Thangavel, R., Lee, Y. S. & Ko, C. H. Ordered mesoporous carbon CMK-8 cathodes for high-power and long-cycle life sodium hybrid capacitors. *Journal of Alloys and Compounds* **743**, 639-645, doi:10.1016/j.jallcom.2018.02.007 (2018).

21 Zhao, J. *et al.* Hierarchical NiMn Layered Double Hydroxide/Carbon Nanotubes Architecture with Superb Energy Density for Flexible Supercapacitors. *Advanced Functional Materials* **24**, 2938-2946, doi:10.1002/adfm.201303638 (2014).

22 Kleitz, F., Choi, S. H. & Ryoo, R. Cubic Ia3d large mesoporous silica: synthesis and replication to platinum nanowires, carbon nanorods and carbon nanotubes. *Chemical communications*, 2136-2137, doi:10.1039/b306504a (2003).

23 Saikia, D. *et al.* A comparative study of ordered mesoporous carbons with different pore structures as anode materials for lithium-ion batteries. *RSC Advances* **5**, 42922-42930, doi:10.1039/c5ra05168a (2015).

24 Yilmaz, E., Yogi, C., Yamanaka, K., Ohta, T. & Byon, H. R. Promoting formation of noncrystalline Li_2O_2 in the Li-O_2 battery with RuO_2 nanoparticles. *Nano letters* **13**, 4679-4684, doi:10.1021/nl4020952 (2013).

25 Xu, S. *et al.* Textile Inspired Lithium-Oxygen Battery Cathode with Decoupled Oxygen and Electrolyte Pathways. *Advanced materials* **30**, doi:10.1002/adma.201704907 (2018).

Acknowledgement

I appreciate Assoc. Prof. Wei Chen, who provides such a precious opportunity to engage in his research lab and train my research skills. Besides, Mr. Yin Zhou, my mentor, guided me and taught me a lot in his field. He shared his experience of being a Ph.D. student, inspiring me to do further researchs as well. Additionally, I want to thank other members in the Surface and Interface Lab for helping me and lighting scientific lamps for me with their encyclopedic knowledges.

I also want to thank the Go Global office and other faculties in both the University of Bitish Columbia and National University of Singapore. They supported me in finance and communicating skills to run this project.

Appendices

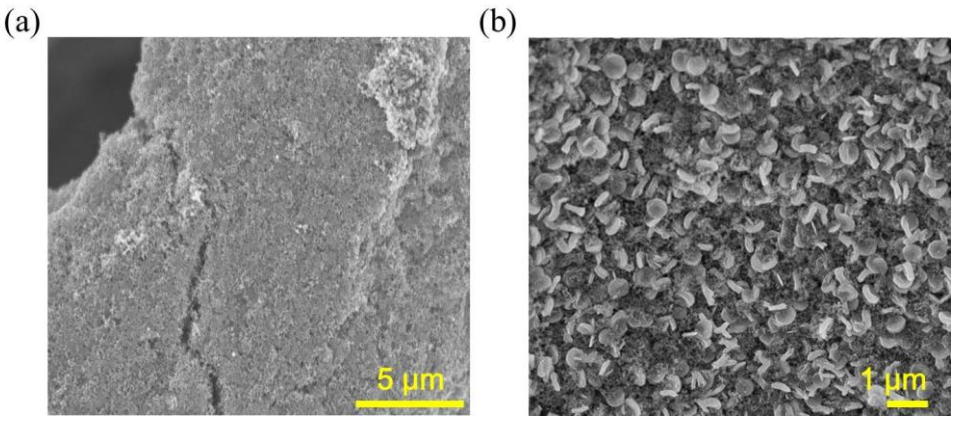

Figure S1. (a) SEM image of the EC-300J cathode before charge; (b) SEM image of a discharged EC-300J electrode at a limited capacity of 500 mAh g-1 at 0.1 A g-1.

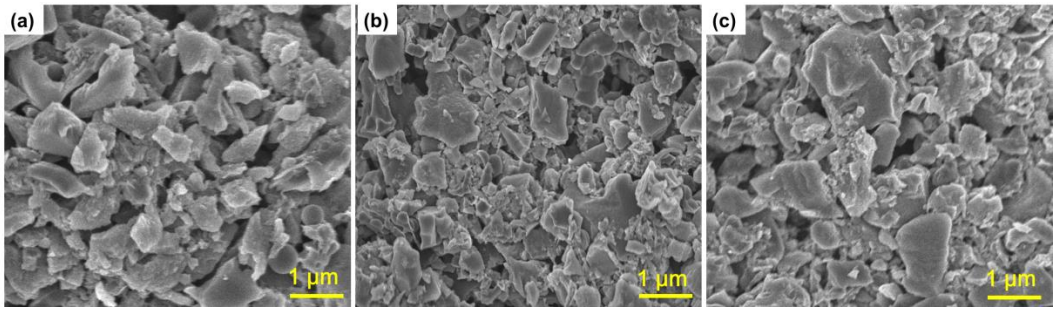

Figure S2. (a) SEM image of the CMK-8 cathode before charge; (b)-(c) SEM images of the discharged CMK-8 electrode at a limited capacity of (b) 500 mAh g-1 and (c) 1000 mAh g-1 at 0.1 A g-1.

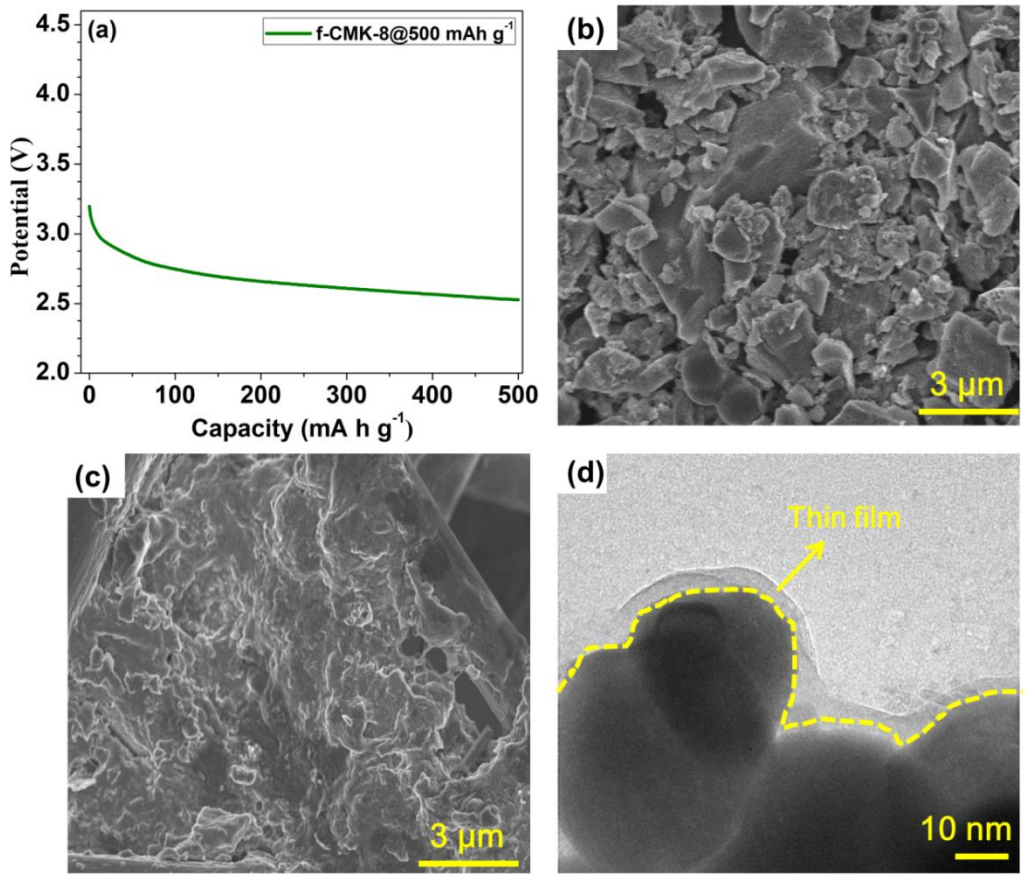

Figure S3. (a) The 1st discharge profile of the f-CMK-8 cathode at 0.1 A g-1 with a limited capacity of 500 mAh g-1; (b) SEM image of the f-CMK-8 cathode before charge; (c)-(d) SEM image and TEM image of a discharged f-CMK-8 electrode at a current density of 0.1 A g-1 with a limited capacity of 500 mAh g-1.

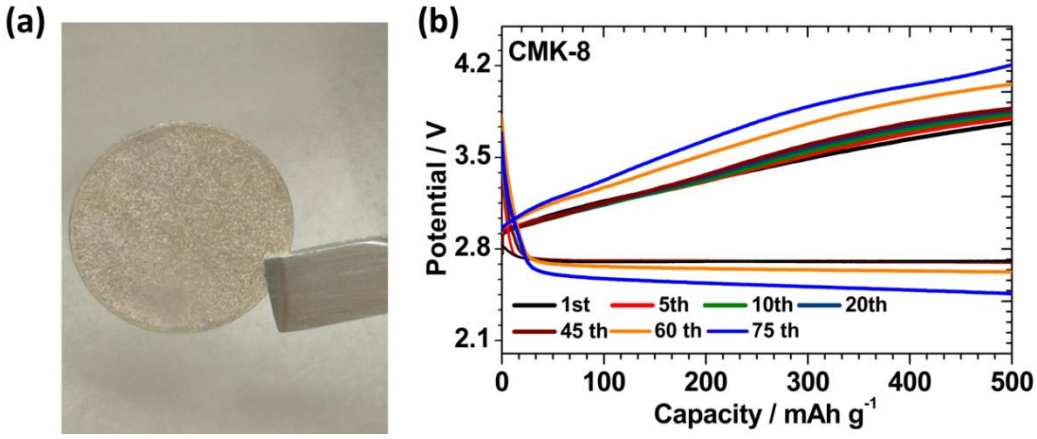

Figure S4. (a) The morphology of lithium anode before charge; (b) the cycle performance of Li-O2 batteries with the CMK-8 cathode at a current density of 0.1 A g-1 with a limited capacity of 500 mAh g-1.

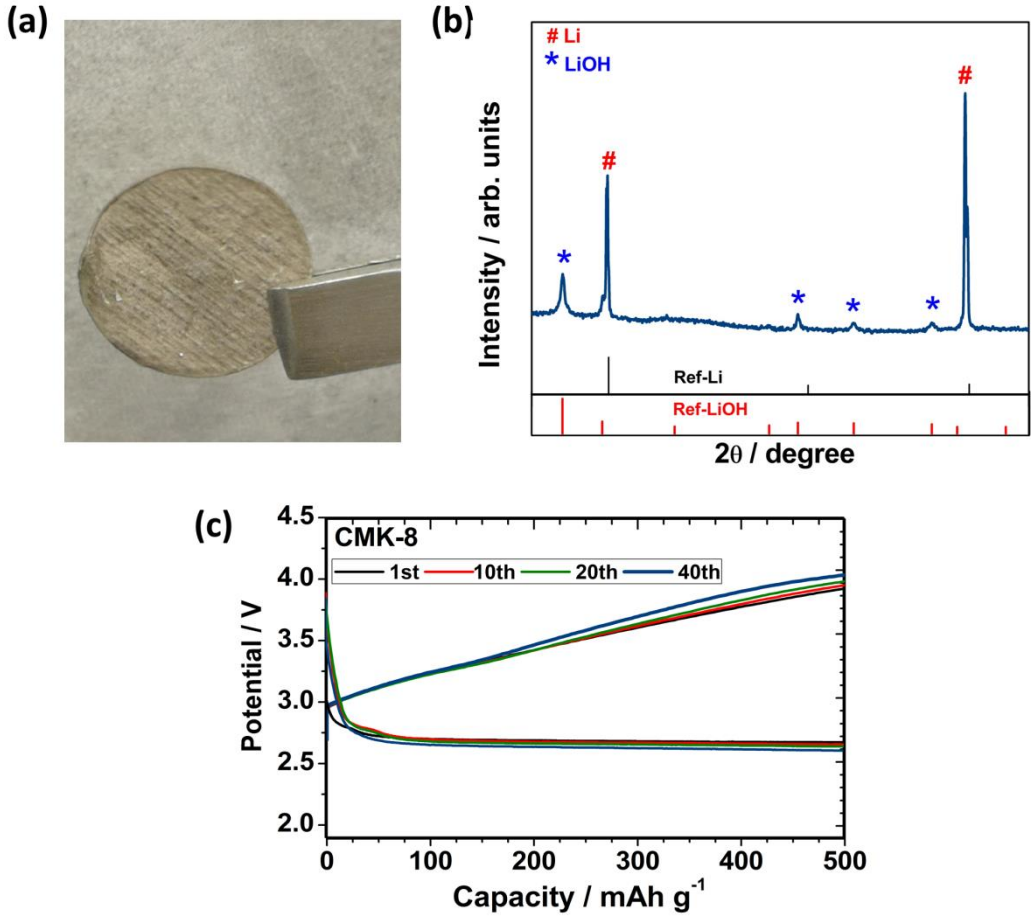

Figure S5. (a) The morphology of the Li metal anode after 75th charge; (b) XRD pattern of the Li metal anode after 75 cycles; (c) the cycle performance of Li-O2 batteries with the CMK-8 cathode after replacement of the Li metal anode with a new one.

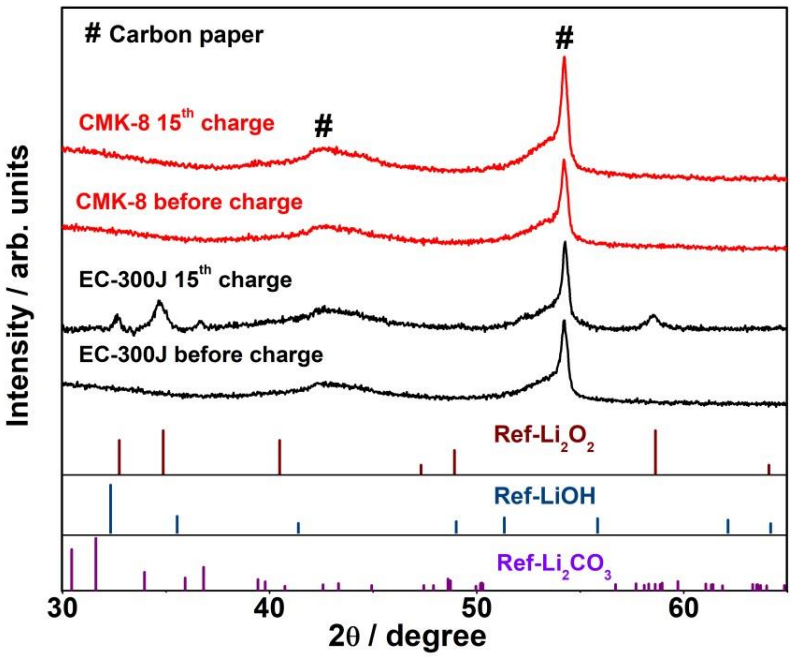

Figure S6. XRD patterns of EC-300J and CMK-8 cathodes before charge and after the 15th charge.